JOURNAL OF APPLIED PHYSICS VOLUME 92, NUMBER 5 1 SEPTEMBER 2002

Uniformity tests of individual segments of interband cascade diode laser Nanostacks®

V. Malyarchuk, J. W. Tomm,[a] and Ch. Lienau
Max-Born-Institut, Max-Born-Strasse 2 A, 12489 Berlin, Germany

M. Behringer and J. Luft
OSRAM Opto Semiconductors, Wernerwerksstrasse 2, 93049 Regensburg, Germany

(Received 20 March 2002; accepted for publication 7 June 2002)

We investigate optoelectronic properties of monolithically stacked diode lasers, so-called Nanostack® devices that include two nominally identical waveguide segments separated by a specially designed tunnel junction. Near-field optical microscopy provides straightforward and separate access to the properties of both optically active segments. Device emission, namely electroluminescence and lasing, as well as photoluminescence and photocurrent data, are recorded with high spatial resolution and consistently interpreted. We find reduced laser emission from the laser segment that is situated closer to the substrate. We show that this is not caused by thermal effects but most likely due to a larger trap concentration within or in the vicinity of the quantum wells of this laser segment. Furthermore, we show that in the unbiased devices the potential gradient in this segment is significantly larger than in the one close to the heat sink. In addition it is shown that the coupling between both waveguides is marginal. The results underline the potential and unique advantages of near-field optical microscopy for nondestructive analysis of optoelectronic device. © *2002 American Institute of Physics.* [DOI: 10.1063/1.1497460]

I. INTRODUCTION

Monolithic diode laser stacks were first proposed several years ago by van der Ziel and Tsang[1] and are practically implemented by several groups.[2–5] In this kind of interband-cascade structures N pn junctions are grown on top of each other. Thus a $(pn)^{\mathrm{N}}$ structure is obtained. Applying an external voltage to this junction stack each second junction is forward biased, whereas the remaining junctions are reverse biased. The resulting unwanted current blocking effective for the whole device can be almost completely canceled by designing the backward biased junctions as specially designed tunnel junctions. This is achieved by introducing extremely high p- and n-doping levels ($\sim 10^{19}$ cm^{-3}) close to the region where the conductivity type inverts. So in this region electrons and holes coexist at similar energy and are spatially separated only by an ultrathin depletion layer. This presents ideal conditions for carrier tunneling. It has been shown that the electro-optical behavior of such stacks scales is almost perfect; i.e., voltage drop and slope efficiency are multiplied by N, whereas the threshold current remains almost unchanged.[2–5] This is maintained up to operation conditions where thermal effects become relevant. Thus such structures rather meet requirements of applications as high-brightness coherent radiation source for pulsed operation conditions. Additional technological advantages are related to the reduced operation currents that need to be provided by the power supply.

Generally, the design of multiple, lateral, and vertical structures such as arrays and stacks is linked to reduced reliability figures. Different kinds of structural inhomogeneity are connected to these designs, e.g., nonequilibrium carrier concentration, light flux, or temperature. Finally this results in an inhomogeneous thermal load. Therefore it is particularly important for monolithic laser stacks to appear either uniform or to compensate for inhomogeneities that are involved in the particular device architecture.

The main topic of this article is a uniformity analysis of monolithic stacked laser structures carried out by near-field optical microscopy (NSOM). We apply three different NSOM-based techniques, namely photoluminescence (PL), photocurrent (PC), and analysis of the laser emission of the device itself. The results allow drawing conclusions regarding the homogeneity of the stacks within the devices.

II. EXPERIMENT

The 808 nm (1.53 eV) emitting high-power laser devices investigated are based on a standard asymmetric large optical cavity (LOC) structure that involves a 1 μm thick $Al_{0.3}Ga_{0.7}As$ waveguide (energy gap, $E_g = 1.8$ eV) and an InAlGaAs double quantum-well (QW) section located inside the waveguide but off centered by 120 nm. The cladding material is $Al_{0.6}Ga_{0.4}As$ ($E_g = 2.2$ eV). A schematic diagram of the spatial variation of E_g is given in Fig. 1(a) on top, cf. Ref. 6. Two such standard structures grown on top of each other and separated by a specially designed tunnel section form the Nanostack® devices are investigated in this study, [see Fig. 1(a) bottom]. Figure 1(b) gives the $L-I-V$ curves for a Nanostack® device together with data of a regular ref-

[a]Author to whom correspondence should be addressed; electronic mail: tomm@mbi-berlin.de

 © 2002 American Institute of Physics

Downloaded 15 Oct 2006 to 62.141.169.136. Redistribution subject to AIP license or copyright, see http://jap.aip.org/jap/copyright.jsp

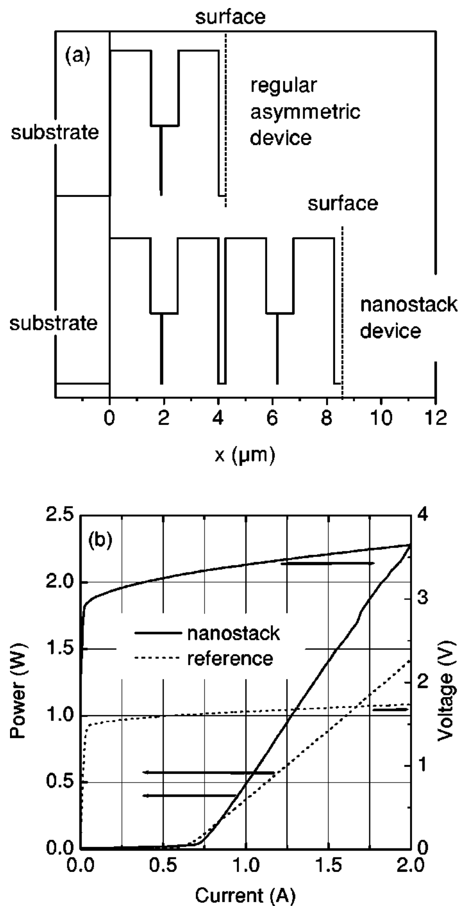

FIG. 1. (a) Diagrams of the spatial variation of E_g along growth direction of the epilayers for a regular asymmetric LOC device (top) as well as for a Nanostack® structure. (b) $L-I-V$ curves for a regular diode laser based on an asymmetric LOC structure and a Nanostack® device.

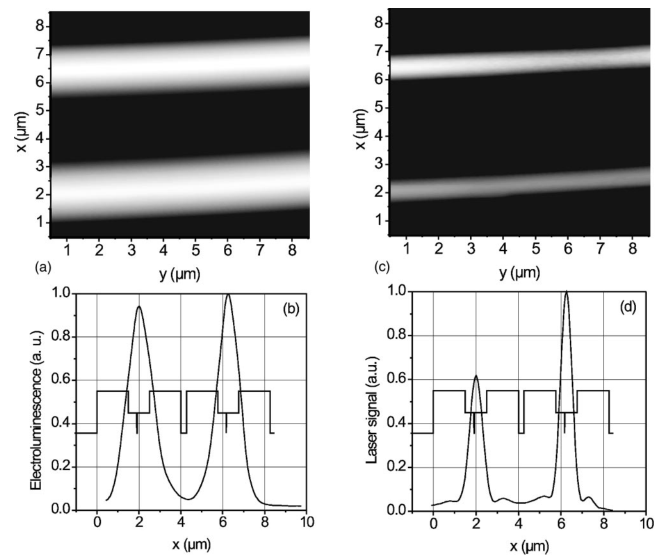

FIG. 2. Electroluminescence (a) and laser emission (c) maps obtained from a Nanostack® device. From such maps we extract linescans that are shown in (b) and (d). The pulsed device operation conditions are for electroluminesence $f=1.22$ kHz, $\tau=410$ μs, and for laser emission $f=1.22$ kHz, $\tau=20$ ns. Thus the integral thermal load is by a factor of 820 lower for the lasing experiment compared to the electroluminescence one.

erence device. The data indicates that the stacked device scales nearly ideally, i.e., voltage drop and slope efficiency double, whereas the threshold current is almost maintained. All investigated Nanostack® devices are from the same wafer and are packaged *p*-side down on standard C mounts in order to secure optimized heat removal from the optically active regions.

The NSOM system used is based on a commercial Topometrix Aurora system. The setup is used in two different operation modes, namely in the luminescence collection and in the excitation mode. All experiments are performed at room temperature. Details of the experimental setup and the near-field techniques employed are described elsewhere.[7–9]

In the collection mode we detect either the electroluminescence or laser emission from the device, operated either below or above threshold, respectively, or the PL signal[7] excited by different excitation sources. We use the 442 nm line of a HeCd laser ($E=2.8$ eV) and a tunable Ti:sapphire system that allows for excitation in the 1.48–1.75 eV range. These lasers are coupled into the fiber. The luminescence is collected trough the same fiber and detection is implemented by a liquid nitrogen cooled charge coupled device camera operating in single photon counting mode or an Si:avalanche photodiode. Thus contributions by diffused carrier pairs are reduced, e.g., compared to PC experiments. This experimental approach ensures a spatial resolution of better than 150 nm. For details, see Ref. 9.

In excitation mode experiments the device itself serves as the detector for the induced PC[8,10] which is fed into the NSOM electronics in the same way as the detector signals in the PL experiments. Under these conditions, compared to the PL experiments, the spatial resolution is poorer. Nevertheless, as demonstrated in Ref. 8, PC structures in diode laser waveguides, separated by 400 nm are clearly resolved as single peaks.

III. RESULTS

Figure 2 shows electroluminescence (a) and laser emission maps (c) obtained from a Nanostack® device. For the electroluminescence measurement the device was operated with 40 mA pulses having a duration $\tau=410$ μs at a repetition rate of $f=1.22$ kHz resulting in a duty cycle of 50%. For the laser emission experiment at 1 A a duty cycle of 0.0024% was chosen ($f=1.22$ kHz, $\tau=20$ ns). Thus despite the increased operation current the integrated thermal load for the laser experiment is reduced by a factor of 820. From such laterally homogeneous maps we extract linescans that are shown in Figs. 2(b) and 2(d) for electroluminescence and lasing, respectively. Obviously there is an asymmetry between the two sections that is even more strongly pronounced for the laser emission experiment. Thermal effects do not account for this as indicated by Fig. 2, taking into account the substantially reduced thermal load in the laser experiment. Extra measurements at different excitation currents confirm this, too.

In order to get more details on the observed asymmetric luminescence behavior we change the luminescence excitation mechanism by switching from electrical to optical excitation, i.e., to a PL experiment. Figure 3 shows PL data for

Downloaded 15 Oct 2006 to 62.141.169.136. Redistribution subject to AIP license or copyright, see http://jap.aip.org/jap/copyright.jsp

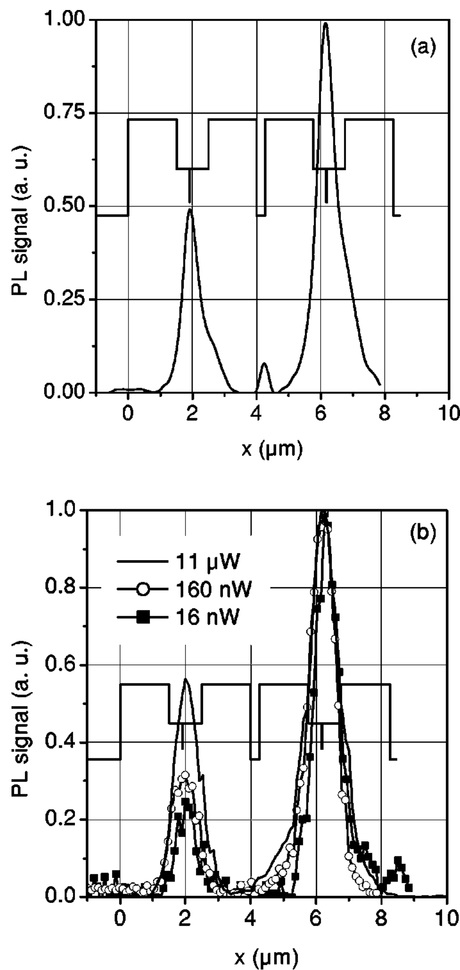

FIG. 3. PL line scans across the Nanostack® laser structure: (a) The excitation energy is 2.8 eV causing surface excitation. Thus the "information depth" in this experiment is exclusively determined by diffusion. The detection window is set to the QW emission photon energy of 1.53 eV. (b) The excitation photons of 1.69 eV energy selectively excite the QW region and become absorbed within about 100 μm (information depth). The detection window is set to the QW emission photon energy of 1.53 eV. The parameter is the excitation power.

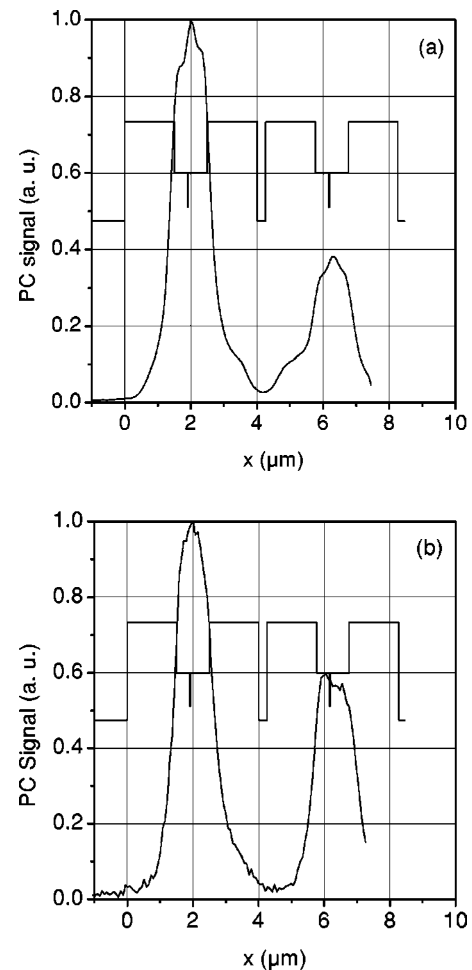

FIG. 4. PC line scans across the Nanostack® laser structure. (a) The excitation resonant to the QW energy is 1.59 eV. The multiple structures are due to the excitation of the three confined waveguide modes (see Ref. 9). (b) The excitation resonant to the QW energy is 2.8 eV causing surface excitation.

two different excitation energies, namely 2.8 eV (a) and 1.69 eV (b). For both experiments the spectral detection window is set to the QW emission energy at 1.53 eV. Excitation with 2.8 eV implements surface excitation for *all* regions of the structure (including the cladding layer) [cf. Fig. 1(b)], whereas the 1.69 eV photons exclusively excite the QWs and the GaAs ($E_g = 1.424$ eV) specially designed tunnel junction region.

Obviously the asymmetric behavior observed in the device emission is also present for external photoexcitation regardless of the QW is directly excited [cf. Fig. 3(b)], or predominantly indirectly populated by carriers generated originally within the waveguide [cf. Fig. 3(a)]. Additionally Fig. 3(b) shows an excitation intensity dependence of the PL emission for exclusive QW excitation. For very low excitation densities the observed asymmetry becomes further enhanced.

Now we present the PC experiments. Data are shown in Fig. 4 and again indicate an asymmetric behavior of the two segments of the stack. For these experiments, however, the stronger response comes from the segment close to the substrate, i.e., the one that shows the poorer luminescence behavior. Furthermore, the asymmetry is less pronounced for surface excitation [2.8 eV, cf. Fig. 4(b)] compared to selective QW excitation [1.59 eV, cf. Fig. 4(a)].

We should mention that the specific shape of the scan excited at 780 nm (1.59 eV) is explained by the mode structure of this particular LOC waveguide design as quantitatively analyzed before for similar waveguides being incorporated into devices with only one waveguide.[8]

IV. DISCUSSION

In order to consistently interpret the data obtained with the different techniques, we summarize in brief the relevant signal generation mechanisms.

(i) The room-temperature QW PL signal is proportional to $\delta n \sim \tau$. Here δn is the nonequilibrium concentration of electron–hole pairs and τ their total lifetime. For very low excitation densities carrier trapping into a finite number of defects might be effective. This results in a reduction of PL intensity at low excitation levels. Moreover trapping and saturation at higher excitation densities and a superlinear dependence of the PL intensity on δn is obtained.

Downloaded 15 Oct 2006 to 62.141.169.136. Redistribution subject to AIP license or copyright, see http://jap.aip.org/jap/copyright.jsp

(ii) The PC signal is proportional to $\delta n \times \mathrm{grad}(V)$, where V is the effective potential experienced by the carrier pairs. V is partly determined by the band gap variation [cf. Fig. 1(a)], but—at the very high doping levels in these devices—doping has an even stronger influence. So large grad(V) values are expected in the depletion layers of the waveguides. The effect of the nominally even larger grad(V) value at the specially designed tunnel junction, however, is likely to be compensated by the tunnel effect itself which results in a suppression of spatial carrier separation and hence in a reduction of the PC contribution from the specially designed tunnel junction. If this would not be the case the junction would not operate properly. Figure 1, however, clearly demonstrates the excellent performance of this crucial device part.

(iii) The electroluminescence as well as the laser signal depend in a very complex way on several parameters, among them also δn and grad(V). Finally, this complexity is the reason why we are not able to restrict our study to the emission properties of both device sections, (cf. Fig. 2). We note that the potential V in the emission experiments differs substantially from the one relevant in (i) and (ii), since the external voltage levels the contribution that originally arises from the doping. The voltage drop across the device [cf. Fig. 1(b)] is a measure of this potential leveling.

First we discuss effects that might be inherent for the specific NSOM experiments. One may argue that the different behaviors of the two segments in Figs. 2–4 arise from the complex twin-waveguide architecture including coupling effects between both laser segments, or reflection at the *p*-contact metallization. The different behavior of PL and PC ratios, where at least the generation process of carrier pairs is similar, is in clear contrast to this interpretation. Second, the PL and PC experiments with high-energy surface excitation (cf. Figs. 3 and 4) show almost the same intensity ratio for the signals from both sections as those experiments for resonant QW excitation, where the three confined waveguide modes (for details cf. Ref. 8) are resolved as clear structures in the spatial PC scans. Thus interference of waveguiding effects on our data can be ruled out, too.

Electroluminescence as well as laser emission show weaker emission intensity from the QW in the device section that is situated closer to the substrate. This could be explained by an increased defect concentration within or in the vicinity of these QWs. The increase of asymmetry in the lasing experiment compared to the electroluminescence is then explained by the nonlinearity of the laser $L-I$ curve.

The PL experiment with exclusive excitation of the QWs within the "bulk" of the waveguide (information depth $\sim$100 μm) [cf. Fig. 3(b)] confirms the assumption of an increased defect concentration within the device section that is situated closer to the substrate by proving that this effect is independent of the generation mechanism. Furthermore, the intensity dependence of the PL indicates a behavior that is indicative for trap saturation within the device section that is situated closer to the substrate.

Independently, the PC experiment provides additional confirmation: If one compares Figs. 4(a) and 4(b) one finds that the asymmetry is less pronounced for surface excitation (2.8 eV). Since grad(V) is almost independent on the depth where δn is created (defined by the excitation energy) this is an indication that the enhanced nonradiative recombination appears rather in the "bulk" of the waveguide than at the surface of the structure. This argument is reasonable since it appears justified to assume that the facet status of both laser segments is similar.

Despite the different signal ratios of both device sections obtained in PL and PC, both sets of data clearly indicate an enhanced recombination efficiency in the QW in the device section next to the substrate. The reduced PL intensity reflects the trapping of carriers into defect states. PC and intensity dependent PL data identify the bulk of the waveguide as the main location of the defects. Thus the assumption of an increased trap concentration in one of the laser segments consistently explains the asymmetric behavior of the laser stack.

V. SUMMARY

We investigate the optoelectronic properties of monolithically stacked high power diode lasers including two nominally identical waveguides separated by a specially designed tunnel junction. NSOM analysis straight and separately addresses the properties of both segments. Device emission, namely electroluminescence and lasing, as well as PL and PC data are recorded and consistently discussed. It is shown that the coupling between both waveguides is marginal.

We find slightly reduced laser emission from the laser segment that is situated closer to the substrate. We show that this is not caused by thermal effects or by effects caused by the complex architecture of the two waveguides but most likely due to a larger trap concentration within or in the vicinity of the QWs of this laser waveguide. Furthermore, we show that in the unbiased devices the potential gradient in this segment is significantly larger than in the one close to the heat sink. The latter effect is not necessarily directly connected to the detected different trap concentration, however, both might be linked to the doping.

These results illustrate the potential of NSOM based optical spectroscopy for nondestructive optoelectronic device analysis in particular if the superior spatial resolution as well as the ability for selective excitation is employed.

ACKNOWLEDGMENTS

The authors would like to thank M. Tischer for expert technical assistance. Financial support by the BMB+F under Contract No. 13N 7384/8 is gratefully acknowledged. Nanaostack® is a registered trademark by OSRAM Opto Semiconductors GmbH. All rights reserved.

[1] J. P. van der Ziel and W. T. Tsang, Appl. Phys. Lett. **41**, 499 (1982).
[2] J. Ch. Garcia, E. Rosencher, Ph. Collot, N. Laurent, J. L. Guyaux, B. Vinter, and J. Nagle, Appl. Phys. Lett. **71**, 3752 (1997).
[3] S. G. Patterson, G. S. Petrich, R. J. Ram, and L. A. Kolodziejski, Electron. Lett. **35**, 395 (1999).
[4] C. Hanke, L. Korte, B. D. Acklin, M. Behringer, G. Herrmann, J. Luft, B. De Odorico, M. Marchiano, and J. Wilhelmi, Proc. SPIE **3947**, 50 (2000).
[5] http://www.osram-os.com/news/news_power.html
[6] V. Malyarchuck, J. W. Tomm, T. Günther, R. Müller, R. Kunkel, C.

Downloaded 15 Oct 2006 to 62.141.169.136. Redistribution subject to AIP license or copyright, see http://jap.aip.org/jap/copyright.jsp

Lienau, and J. Luft, Proc. SPIE **4287**, 111 (2001).
[7] C. Lienau and T. Elsaesser, Semicond. Semimetals **67**, 39 (2001).
[8] T. Guenther, V. Malyarchuk, J. W. Tomm, R. Müller, and Ch. Lienau, Appl. Phys. Lett. **78**, 1463 (2001).
[9] V. Emiliani, F. Intonti, C. Lienau, T. Elsaesser, R. Nötzel, and K. H. Ploog, Phys. Rev. B **64**, 155316 (2001).
[10] A. Richter, J. W. Tomm, Ch. Lienau, and J. Luft, Appl. Phys. Lett. **69**, 3981 (1996).

Downloaded 15 Oct 2006 to 62.141.169.136. Redistribution subject to AIP license or copyright, see http://jap.aip.org/jap/copyright.jsp